A Refraction-Diffraction Model for Irregular Waves

Q. Gao[1], A.C. Radder[2]

Abstract

A numerical model for wave refraction and diffraction has been used to compute irregular waves. The model is based on the parabolic approximation, but, by combining with the perfect boundary condition, it is suitable for waves propagating with large incident angles. The irregular waves are modelled through linear superposition of wave components. In order to apply the model to field cases, however, the numerical computations were carried out with one representative frequency while retaining spectral representation of the directionality of waves. This approximation has been examined by the laboratory conditions of Vincent & Briggs; The model's performances in the field cases were also investigated.

Introduction

Recently, two distinct wave models have been used to determine wave properties in two-dimensional near shore zones. One is the so-called parabolic wave model based upon the mild-slope equation, the other is the phase averaged model based on the balance equation for wave energy or wave action. Both models are implemented according to Eulerian approach of wave propagation and wave information is available at the mesh-points of a regular grid. The phase averaged model (for example see Holthuijsen et al. 1989, Holthuijsen et al. 1993), if fully discretized in frequency and direction domain, can trustworthy account for various physical processes such as wave generation, dissipation and nonlinear wave-wave interaction. While this greatly improves representation of the random, short-crested waves, the absence of diffraction in the governing equation can lead to inaccuracy in the case of waves with small directional spreading. The parabolic model (see, for example, Radder,1979, Kirby & Dalrymple, 1983) not only contains the processes of wave transformation such as shoaling, refraction and diffraction, but also can include various other physical influences such as wave growth and dissipation (see Vogel et al. 1988), and the model can be easily implemented on nearshore area. However, the parabolic model has its inherent shortcomings: waves must propagate in one

[1] Researcher, Rijkswaterstaat, Institute for Inland Water Management and W&W Treatment/RIZA, Postbus 17, 8200AA, Lelystad, The Netherlands

[2] Senior Researcher, Rijkswaterstaat, National Institute for Coastal and Marine Management/RIKZ, Postbus 20907, 2500EX, The Hague, The Netherlands

principal direction, say x-direction, since the diffraction effect is restricted to y-direction; and the model deals only with regular waves. A numerical model for irregular waves has been developed which is based on the parabolic approximation and which is suitable for waves with large incident angle (see Gao et al. 1993). In the model a careful treatment of the lateral boundary condition was introduced to prevent the contamination from undesirable side effects (see also Dalrymple & Martin, 1992), it not only makes computation very efficient, but also leads the physical interpretation of the computed results straightforward.

The model has been applied to the laboratory cases with fully spectral form. The results compare well with the experiment of wave transformation over the elliptical shoal carried out by Vincent & Briggs(1989), which usually can not be handled properly by a phase averaged model. When the model is applied to the field cases, the computer effort will be very excessive. We will define a representative frequency, mean frequency of waves, instead of full discretization in frequency domain, while the spectral representation of the directionality of waves is still retained as we consider on the coastal area the directional spreading of waves more important than the spectral representation in the frequency domain. The improvement of the model has been found when it was applied to estuary Haringvliet (a closed branch of the Rhine estuary). The model has also been applied to the tidal area of Friesche Zeegat.

Model Equations

In case of an irregular wave field we consider wave components which make fairly large angle θ with the x-direction. The wide angle equation, that describes the transformation of wave potential $\phi(x, y)$, can be derived

$$\left[1-\frac{\varepsilon^2}{2}+\frac{\varepsilon^2}{2k^2}\frac{\partial^2}{\partial y^2}\right]\frac{\partial \phi}{\partial x}=ik\sqrt{1-\varepsilon^2}\left[1+iP_\varepsilon+\frac{1+\varepsilon^2}{2k^2}\frac{\partial^2}{\partial y^2}\right]\phi \qquad (1.a)$$

$$with \quad P_\varepsilon \equiv \frac{1}{2k^2}\left[\sqrt{1-\varepsilon^2}\frac{\partial k}{\partial x}+\varepsilon\frac{\partial k}{\partial y}+\frac{\omega_r}{c c_g}\left(\gamma_d+\nabla\bullet\vec{U}\right)\right] \qquad (1.b)$$

where $\varepsilon=sin\theta$; γ_d is the dissipation coefficient of waves and $\vec{U}$ is the horizontally varying current; c, c_g and ω_r are respectively wave phase velocity, group velocity and relative frequency; wave number k can be calculated according to the linear dispersion relation. The relative frequency is related to the absolute frequency ω by

$$\omega=\omega_r+\vec{k}\bullet\vec{U}, \qquad \omega_r=\sqrt{gk\tanh kh} \qquad (1.c,d)$$

and the local effective depth

$$h(x,y)=d(x,y)+p_a\bullet H(x,y), \quad 0\le p_a\le 1 \qquad (1.e)$$

with $d(x,y)$ indicating water depth and $H(x,y)$ wave height. The dissipation coefficient γ_d can be easily represented, as formulated by Dingemans(1985) and Vogel et al. (1988). If the incident angle θ=0 and if there are no dissipation and current, eq.(1) is then reduced to the eq.(17) of Radder(1979).

Numerical representation of eq.(1) is the discretization of wave potential ϕ in spatial domain (x,y), with $x>0$ and $0<y<y_b$. The discretization in a computational region forms $M+1$ rows in x-direction, with $x_m=m\bullet\Delta x$ (m=0, 1, ...M), and $N-1$ columns in y-direction, with $y_n=n\bullet\Delta y$ ($n=1,2, ...N-1$). The equations for lateral boundaries have to be applied at $n=0$ and $n=N$, to provide enough equations to solve for unknown $\phi_{m,n}$. The solution of $\phi_{m,n}$ is using the Crank-Nicolson method, which is an implicit scheme with second-order accuracy in both Δx and Δy. The details can be found in Gao et al. (1993).

The model has no difficulty to compute two-dimensional spectral waves, with four independent variables x, y, θ and f. The only one dependent variable is wave potential $\phi(x_m, y_n, \theta_i, f_j)$. The computation is as follows: one starts computation at up-wave boundary where $x=0$ and processes in x-direction, the computation in θ-f domain is that one first solves the linear system of one component on a line in y-direction, then processes to next component. The computation can proceed to the next line only after that all wave components in θ-f domain of a line have been determined.

As mentioned, a parabolic wave model requires lateral boundary conditions. An improper treatment of boundary can cause contamination in the computational domain. Therefore, a parabolic model requires a very large computational domain to avoid the contamination of the interesting area from the lateral boundaries, which leads to inefficiency in computation. A perfect transmitting boundary condition (see also Gao et al. 1993; Dalrymple & Martin, 1992) has been established to allow waves to transmit out or into the computational domain without reflection regardless its direction, crest curvature and the strength of the scattering.

The basis for such a boundary condition is that an exact description of waves in the shadow regions (outside of the computational domain) has to be obtained. To this end we assume in these regions that bottom has straight and parallel contour lines to y-direction and that wave dissipation depends only on x, then eq.(1) can be solved analytically for wave potential ϕ. In practice, we use the differential form of wave potential at the lateral boundaries rather than an analytical one in order that it can be combined with the discretized form of eq. (1). The following equation, which is discretized in x-direction, can be derived

$$\frac{\partial \phi}{\partial y}^{m} + k\sigma\,\phi^{m} = \frac{\partial \phi_{inc}}{\partial y}^{m} + k\sigma\,\phi_{inc}^{m} + k\sum_{\iota=0}^{m-1}\rho_{\iota}\left(\phi^{\iota} - \phi_{inc}^{\iota}\right) e^{i\sum_{\iota}^{m} k\delta(x_{\iota})\Delta x} \qquad (2)$$

which is consistent with the discretized form of eq. (1) at the boundaries. Eq.(2) is the so-called perfect transmitting boundary condition, where ϕ_{inc} is the incident wave which can be obtained numerically, coefficients σ, ρ and δ are given as follows:

$$\delta(x) = \frac{\sqrt{1-\varepsilon^2}}{1-\frac{\varepsilon^2}{2}}\left(1+iP_\varepsilon\right), \qquad \sigma = -i\frac{I}{\sqrt{\beta}}e^{i\mu}\left[J_o(\mu) - iJ_1(\mu)\right] \tag{2.a,b}$$

$$\beta = \frac{\varepsilon^2}{1-\varepsilon^2/2}, \qquad \rho_0 = -i\frac{I}{\mu\sqrt{\beta}}\left[Q(m\mu) - Q((m-1)\mu)\right] \tag{2.c,d}$$

$$\rho_\iota = -i\frac{I}{\mu\sqrt{\beta}}\left[2Q((m-\iota)\mu) - Q((m-\iota+1)\mu) - Q((m-\iota-1)\mu)\right] \tag{2.e}$$

with

$$\mu = \frac{1-\varepsilon^2/2}{\varepsilon^2/2}\frac{\sqrt{1-\varepsilon^2}}{4}\left[\frac{1-\varepsilon^2(1+\varepsilon^2)/2 - i\varepsilon^2 P_\varepsilon}{(1-\varepsilon^2)^2}\right]\Delta x\left(k + \int\frac{\partial k}{\partial x}dx\right) \tag{2.f}$$

$$Q(z) = ze^{iz}\left[J_o(z) - iJ_1(z)\right] \tag{2.g}$$

in which $I=+1$ for left hand side boundary where $y=y_b$ and $I= -1$ for right hand side one where $y=0$, J_0 and J_1 being respectively the zero- and first-order Bessel function. Combining the discretized form of eq.(1) with eq.(2) results a linear system with tridiagonal matrix, which can be solved very efficiently.

To illustrate the performance of the perfect transmitting boundary condition, we compared the numerical results of eq.(2) with a simple absorbing boundary condition, given by

$$\cos\theta\frac{\partial\phi}{\partial x} + \sin\theta\frac{\partial\phi}{\partial y} = ikp_s\phi \tag{3}$$

where θ is the angle at which the plane waves propagate and p_s is taken to be 1. A test was carried out for monochromatic waves in water a basis of $500m \times 500m$, with water depth decreasing from $10m$ at $x=0$ to $5m$ at $x=500m$. The incident waves have height 1 meter, period 8s and an angle 30^o with x axis. The spatial resolution is $\Delta x=5m$, $\Delta y=7.5m$. In figure (1a) the computation was carried out with eq. (2) to be applied at both boundaries. The robustness of eq.(2) can easily be seen in left panel of figure 1, where waves are reasonably calculated across the whole computational line. Whereas in figure (1.b) we apply eq.(3) to $y=0$, the boundary of outgoing waves, the distortion in wave field can be easily found.

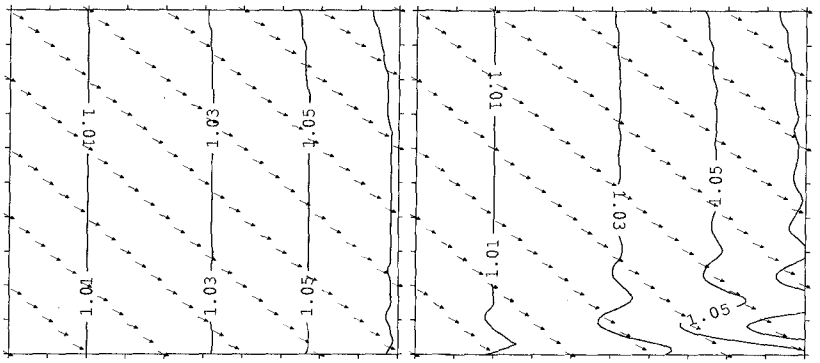

Figure 1. The plane waves propagate at *30°* angle over a shoaling bottom, where arrows indicate the angle at which the waves propagate, and solid line is the iso-line of wave height.

Comparison with The Results of Experiments by Vincent & Briggs

Vincent & Briggs (1989) carried out experiments to simulate regular and irregular random waves in a hydraulic model, which consists of an elliptical shoal and an array of wave sensors. For details of the experiments the reader is referred to Vincent & Briggs. The incident waves which were generated by the spectral wave maker are described by TMA spectrum

$$E(f) = \alpha\, g^2 (2\pi)^{-4} f^{-5} \exp\{-1.25(\frac{f_p}{f})^4 + \ln\gamma \exp[-\frac{(f-f_p)^2}{2\sigma^2 f_p^2}]\}\phi_d$$
$$with\ \ \sigma = \sigma_a = 0.07 \ \ if\ f \le f_p, \quad \sigma = \sigma_b = 0.09 \ \ if\ f \ge f_p; \tag{4.a}$$

where α is the Phillip's constant, f_p the peak frequency, γ the peak enhancement factor, σ the wave shape factor. The shallow water factor ϕ_d is given by

$$\phi_d = 0.5\omega_d^2, \ \ if\ \omega_d < 1; \qquad \phi_d = 1 - 0.5(2-\omega_d)^2, \ \ if\ 1 \le \omega_d \le 2$$
$$\phi_d = 1, \qquad if\ \omega_d > 2; \quad with \quad \omega_d = 2\pi f\sqrt{h/g} \tag{4.b}$$

The directional spreading used in the experiments is the Fourier series representation for the wrapped normal function, which will be approximated in our computations by the following one

$$D(\theta_i) = \frac{1}{2I_s}\cos^s(\theta_i - \theta_o), \quad with \ \ I_s = \int_0^{\pi/2}\cos^s(\theta)d\theta \tag{5}$$

where s is the directional spreading parameter, $\sigma_m = 10$ of the Fourier representation for the directional spreading will be approximated by $s=20$ of eq.(5) and $\sigma_m = 30$ by $s=4$.

A very high resolution in θ-f domain requires excessive computer effort when the model is applied to field cases. To this end, an approximation will be introduced and the accuracy of it will be examined. We are going to define a representative frequency, mean frequency, to approximate the full discretization in frequency domain, while the spectral representation of directionality of waves will be retained. This can not only save the computational cost by one order or more, but also allow us to employ the expressions for wave dissipation and wave growth in the model easily. The representative period is defined as follows

$$f = \frac{1}{E_o} \int f\, E(f)\, df, \quad T = 1/f \ \text{ with } \ E_o = \int E(f)\, df. \tag{6}$$

To examine the performance of this approximation, we compare to the laboratory case N1 and B1 of Vincent & Briggs, where case N1 and B1 have respectively a narrow and broad directional spreading. For each case three computations were carried out with the numerical model. The first computation was carried out with fully spectral form; the frequencies vary from the minimum f_1=0.5Hz to the maximum f_{15}=1.5Hz, with Δf=0.071; the directional sector is 120^o and angular resolution is $\Delta\theta=5^o$ for all cases. The second and third computations were carried out with or without dissipation due to wave breaking; we employ the approximation form of eq.(6), but still keep the directionality of the spectral waves. There are total 15×25=375 wave components per mesh point in the first computation and only 25 in the second and third computation. The input parameters are listed in table 1. The parameters in column 2, 3, 4, 5, 7 and 8 are those used in the first computation and those in column 2, 6 to 8 are used in the second or third computations. The computation consists an area of 20m by 23m and the numerical resolution in spatial domain is $\Delta x=0.1m$, $\Delta y=0.1m$.

case	H(cm)	T_p(s)	α	γ	T(s)	s(eq. 5)	p_a
N1	7.75	1.3	0.0144	2	1.07	20	0.5
B1	7.75	1.3	0.0044	2	1.07	4	0.5

Table 1 The parameters used by the numerical model.

From above computations the following points are to be worthily noted.

1. The model computes the waves in fully spectral form (discretized in both frequency and directional domain) of the laboratory situation with reasonably accuracy and small cpu cost (about 15 minutes on Pentium 90).
2. We find that the differences between the wave heights calculated by the fully spectral form and by the approximation form of eq.(6) are insignificant.
3. Along section 3 discrepancies are found between the computed and measured wave heights in the divergence zones, but the differences decrease for waves with the broad directional spreading.
4. Along section 7-9 of wave propagation direction, the computed and measured wave heights agree reasonably well.
5. It is not conclusive that one can improve the computed results by including wave dissipation in the model.

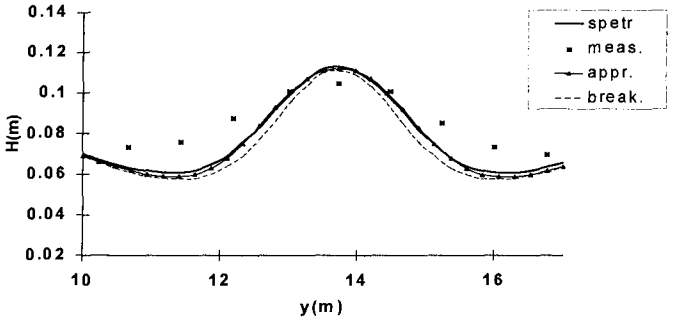

Figure 2a. Comparison between the computed and measured wave heights along the section 3 for case N1. The legends are given as follows: spetr: wave heights computed with fully spectral form; meas: measured heights; appr: computed with the approximation of eq. (6); break: computed with dissipation due to wave breaking.

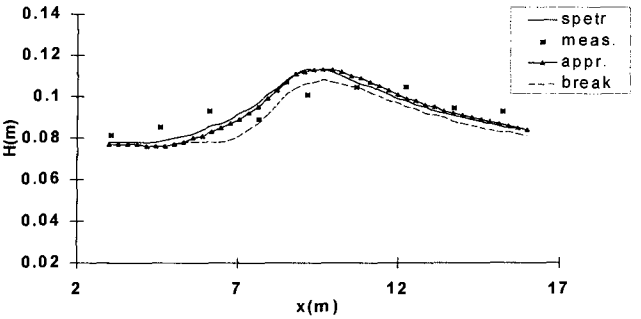

Figure 2b. Along section 7-9 for case N1.

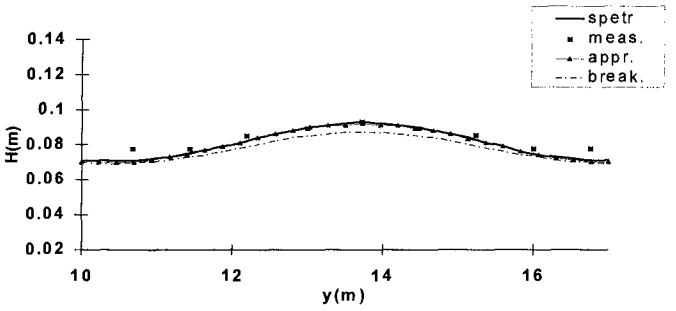

Figure 2c. Along section 3 for case B1.

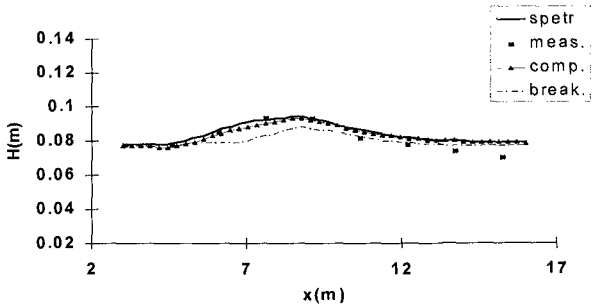

Figure 2d. Along section 7-9 for case B1.

Comparison with Field Measurements

When approaching the shore region, the surface waves will be influenced by a number of factors. Except for wave shoaling and breaking, refraction and diffraction, wind will have a profound effect on waves in a region behind an island or breaker zone. In our model we adopt an empirical expression to account for wave growth due to wind effect(see also Vogel et al., 1988)

$$\gamma_{gr} = -\frac{2c_g}{\tilde{H}_s}\frac{d\tilde{H}_s}{dx}\cos(\theta_w - \theta), \qquad (7)$$

$$with \quad \tilde{H}_s = b\left(1 - \frac{1}{\left(1 - a\sqrt{\tilde{x}_w}\right)^2}\right), \quad and \quad \tilde{H}_s = \frac{gH_s}{U_w^2}, \quad \tilde{x}_w = \frac{gx_w}{U_w^2}$$

where H_s is the significant wave height, U_w, θ_w, θ and x_w are respectively wind speed and direction, wave direction and fetch, coefficient $b=0.30$ and $a=0.009$ were used in the following computations. As mentioned in the previous section we will use a representative period, the mean period, but still keep the directionality of spectral waves in the field cases of the estuary Haringvliet and tidal area Friesche Zeegat.

A. The estuary Haringvliet

The area was chosen to test the model because the wave data in this area is well documented (for details see Andorka Gal, 1995), and because the data set has been extensively used to test the performance of various wave models (see, for example, Vogel et. al, 1988, Holthuijsen et. al,1989). The bathymetry of the estuary and the locations of the measurement are shown in figure 3. The computational area of the present model, which consists of an area of $13600m \times 12400m$, is considerably smaller than those mentioned; the directional sector is 120°. The spatial resolution is $\Delta x=5m$, $\Delta y=10m$ and the angular resolution is $\Delta\theta=15°$, the directional spreading parameter is $s=4$ for all cases. There are total 9 wave components involved in one mesh point. The computations were carried out for the storm situation of 14-15 Oct. 1982. The directional wave buoy WAVEC (see figure 3 at location WA) provides significant wave height, mean wave direction and mean period as up-boundary

conditions; these are listed in Table 2, along with wind and water level. The measured wave heights at other locations were used to check the accuracy of the model. The comparison between the computed and the measured wave heights are given in Table 3. Further the computed wave heights versus the measured ones are shown in figure 4.

	No.1	No.2	No.3	No.4	No.5	No.6
Date/Time	17:00, 14	20:00, 14	22:00, 14	23:00, 14	02:00, 15	04:00, 15
U_w (m/s)	14	14	15	15	13	13
θ_w (degree)	310	310	310	310	310	310
Water level	-0.1m	0.2m	0.85m	1.75m	1.50m	0.45m
H_s(m)	2.58	3.06	3.23	3.54	2.89	2.72
$\overline{T}$(s)	6.0	6.8	6.7	6.7	6.6	6.3

Table 2. The input parameters of the model.

	No.1		No.2		No.3	
	H_{MEAS}	H_{CMP}	H_{MEAS}	H_{CMP}	H_{MEAS}	H_{CMP}
WA	2.58	-	3.06	-	3.23	-
WR1	2.34	2.55	2.65	2.96	2.90	3.13
WR2	2.21	2.17	2.38	2.34	2.53	2.58
WR3	2.21	2.05	2.45	2.28	2.70	2.50
WR4	0.40	0.43	0.48	0.49	0.62	0.56
WR5	0.66	0.79	0.75	0.84	1.05	1.06
WR6	1.16	1.09	1.20	1.28	1.60	1.61
E-75	0.61	0.57	0.74	0.79	0.94	0.95
	No.4		No.5		No.6	
	H_{MEAS}	H_{CMP}	H_{MEAS}	H_{CMP}	H_{MEAS}	H_{CMP}
WA	3.54	-	2.89	-	2.72	-
WR1	3.10	3.40	2.68	2.84	2.49	2.66
WR2	2.63	2.88	2.75	2.67	2.41	2.35
WR3	2.72	2.70	2.68	2.47	2.56	2.24
WR4	0.72	0.80	0.70	0.71	0.44	0.46
WR5	1.45	1.36	1.15	1.26	0.70	0.93
WR6	1.86	1.71	1.95	1.61	1.35	1.32
E-75	1.08	1.08	0.88	0.90	0.63	0.72

Table 3. Comparison of the measured and computed wave heights in Haringvliet.

To measure the performance of the model, we employ the following two statistical expressions, by which the larger waves can not dominate the error quantities; the first one is the relative root-mean-square-error, the second is the performance rate of the model, defined as follows:

$$\varepsilon_{rms} = \sqrt{\frac{1}{N}\sum_{i=1}^{N}\left(\frac{H_{CMP}}{H_{MEAS}} - 1\right)^2}; \quad P_{mdl} = 1 - \frac{\sum_{i=1}^{N}\left(H_{CMP} - H_{MEAS}\right)^2}{\sum_{i=1}^{N}\left(\left|H_{CMP} - \overline{H}_{MEAS}\right| + \left|H_{MEAS} - \overline{H}_{MEAS}\right|\right)^2} \qquad (8.a,b)$$

where H_{CMP} is the computed wave height and H_{MEAS} the measured one, H_{MEAS} is the measured mean wave height. For the data set listed in Table 3 we have ε_{rms}=0.094 and P_{mdl}=76%, these compare favourably to the model CREDIZ(Vogel et al., 1988), which has ε_{rms}=0.17 and P_{mdl}=67%.

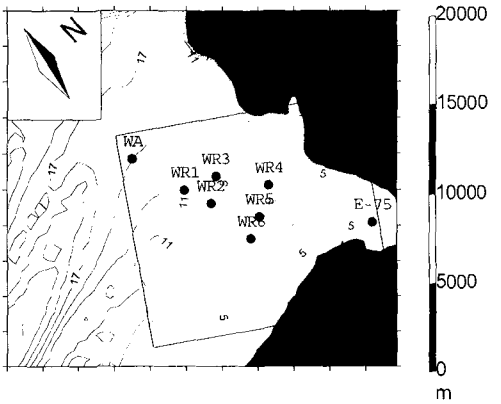

Figure 3 Bathymetry of the estuary Haringvliet and locations of the measurement, where the rectangle indicates the computational area.

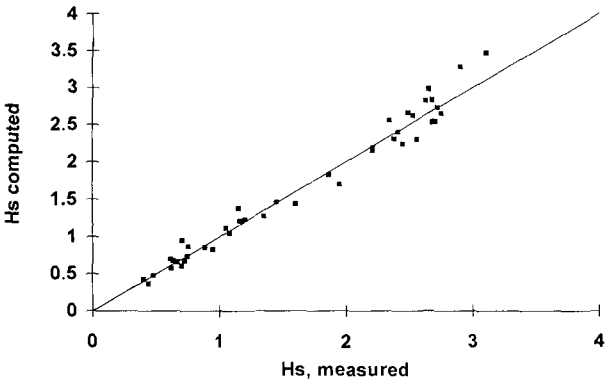

Figure 4 Computed wave heights versus measured ones.

B. The tidal area Friesche Zeegat

The aim is to test the model in a situation of strong tidal current, up which waves propagate. The area was chosen because the wave data from measurements is available (see Dunsbergen, 1995), and tidal currents were calculated with a fair degree of detail. The bathymetry of the area, along with locations of measurement, is shown in figure 5. A shoal, located in the centre of the tidal channel, will shelter most onshore area from the incoming waves. The tidal current, as shown in figure 6a (for

flood case) and figure 7a (for ebb case), will also contribute to deflect the propagation direction of the incoming waves.

The weather situation was that a storm in the North Sea generated waves, which propagated into tidal area. The computations were carried out for the flood case at 06:00 M.E.T., Oct. 9, 1992 and the ebb case at 12:00 M.E.T. Oct. 9 1992 in a rectangular area of 22000m×16000m, the directional sector was taken to be 90°. The waves measured by WAVEC buoy at location **S** is used to provide the model with the up-wave boundary. The input parameters are given in Table 4, where the mean wave direction is the same as wind and is in nautical convention. The wave heights measured at other locations were used to check the performance of the model. The resolution was $\Delta x=5m$, $\Delta y=10m$ and $\Delta\theta=15°$, the directional spreading parameter s=6 is used for flood case and s=10 for ebb case. In these computations only 7 wave components per mesh point are used.

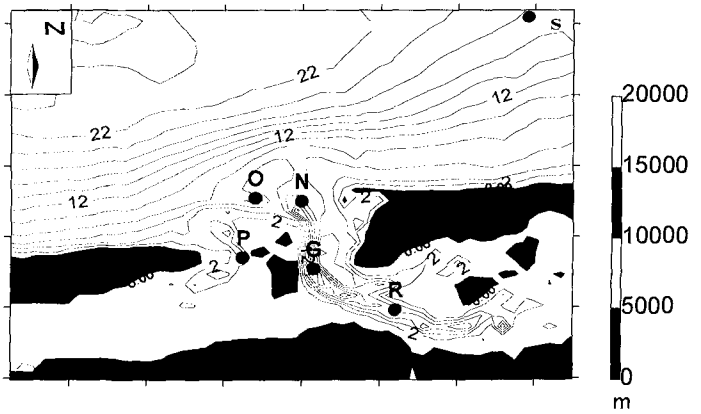

Figure 5 Bathymetry of tidal area Friesche Zeegat with the locations of observation (marked with ●).

	H_s	$\bar{T}$	Water level	U_w	θ_w	s
Flood	2.24	5.6	1.13m	12.0m/s	320°	6
Ebb	3.31	7.4	0.1m	11.5m/s	340°	10

Table 4. The input parameters for the numerical model.

location	N	O	P	G	R
Flood					
H_{MEAS}	1.75	1.90	0.56	0.53	0.31
H_{CMP}	1.72	1.82	0.43	0.40	0.53
Ebb					
H_{MEAS}	1.65	2.62	0.39	0.52	0.43
H_{CMP}	1.94	1.93	0.58	0.59	0.42

Table 5 The measured and computed wave heights for ebb and flood cases.

The comparison between the computed and measured waves is shown in table 5. For the flood case the rms error ε_{rms} is 0.23, the performance rate P_{mdl} is 97% and for the ebb case ε_{rms}=0.27, P_{mdl}=69%. The computed wave fields are shown in figure 6b for the flood case and figure 7b for the ebb case. The following remarks are added here according to the computed results: The varying depth in the area of the tidal inlet deflects the propagation direction of the incoming waves, making them towards the shallow area. In such a situation it is hardly possible for monochromatic waves to penetrate through the channel and to arrive in the onshore region (south of tidal inlet). The eomputations also indicate that in the inlet region the tidal current has profound influence on the computed waves, whereas wind nearly dominates the waves in onshore region.

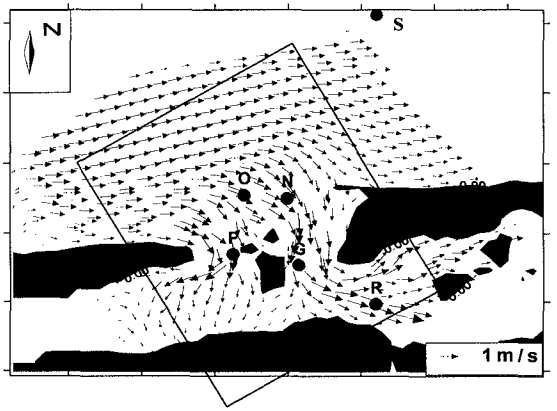

Figure 6a. Tidal current for flood case at 06:00 M.E. T., Oct. 9, 1992 in the area of Friesche Zeegat, where the rectangular line indicates the computational area.

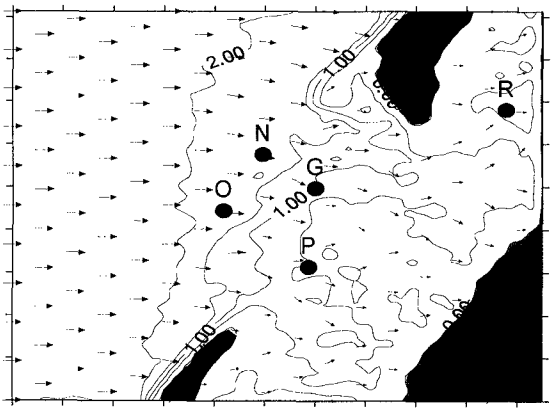

Figure 6b. Computed waves for the flood case, where the iso-lines refer to the wave height and arrows indicate the mean wave direction.

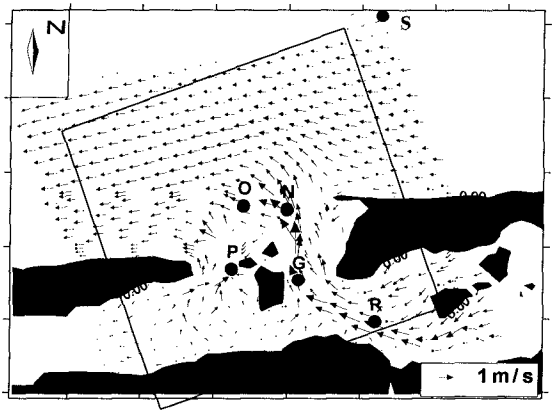

Figure 7a. Tidal current (ebb case) at 12:00 M.E.T. Oct. 9, 1992.

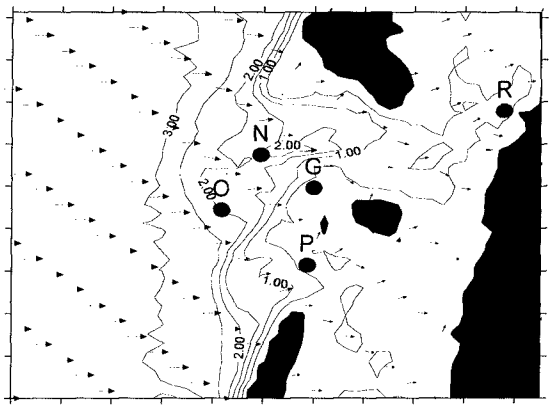

Figure 7b. Computed waves for the ebb case, caption is the same as figure 6b.

Conclusions

The advantage of the parabolic model is that it can be used to compute wave transformation in a large horizontal domain, say, a region of several hundreds of wave length on one side. But when applied to field cases, the model often assumes the incoming waves to be monochromatic. The numerical model presented in this paper can be used to compute irregular waves and regular waves as well. The numerical results have been compared to a number of measurements from hydraulic models as well as field cases on coastal areas. We have the following conclusions: 1, The results show that the model is suitable for waves with large incident angle. 2, Through the linear superposition of regular waves, the model can be used to compute irregular waves; the performance of the model was reasonably good when it was applied to the laboratory cases of Vincent & Briggs. 3, The perfect boundary condition used in the numerical model can allow waves to transmit out or into the computational domain

without causing disturbances in the computational domain, which also makes the computation of waves very efficient. 4, The model can be used to compute waves in field cases and it performs quite well when compared to the observations.

References

Andorka Gal, J.H. 1995. Verification set Haringvliet, Oct. 14, 1982 - Oct. 15, 1982, *Rep. RIKZ-95.112x, Ministry of Transport and Public Works, The Netherlands.*

Dalrymple, R.A. and Martin, P.A. 1992. Perfect boundary conditions for parabolic water-wave models. *Proc. R. Soc. Lond.* A437, pp. 41-54.

Dingemans, M.W., 1985. Surface wave propagation over an uneven bottom. Evaluation of two-dimensional horizontal wave propagation models. *Report W301 part 5, Delft Hydraulics Laboratory* (December 1985).

Dunsbergen, D. W., 1995. Verification set Friesche Zeegat. Oct. 1, 1992 - Nov. 17, 1992, *Rep. RIKZ-95.035, Ministry of Transport and Public Works, The Netherlands.*

Gao, Q., Radder, A.C. and Booij, N. 1993. A numerical wave model for the refraction and diffraction of irregular waves, Description of the wave model CREON. Report 5-93, *Faculty of Civil Engineering, Delft University of Technology, The Netherlands.*

Holthuijsen, L. H., Booij, N., and Herbers, T.H.C., 1989. A prediction model for stationary, short-crested waves in shallow water with ambient current. *Coastal Eng.* 23, pp. 23-54

Holthuijsen, L. H., Booij, N., and Ris, R. C., 1993. A spectral wave model for the coastal zone, *Proc. of 2nd Int. Symposium on Ocean Wave Measurement and Analysis,* New Orleans, 630-641

Kirby, J.T. and Dalrymple, R.A., 1983. A parabolic equation for the combined refraction-diffraction of Stokes waves by mildly varying topography. *J. Fluid Mech.*, 136, pp. 453-466

Radder, A.C., 1979. On the parabolic equation method for water-wave propagation. *J. Fluid Mech.* 95(1), pp. 159-176

Ris, R.C. 1997. Spectral modelling of wind waves in coastal areas. *Ph.D. dissertation, Faculty of Civil Engineering, Delft University of Technology, The Netherlands.*

Vincent, C.L. and Briggs, M.J. 1989. Refraction-diffraction of irregular waves over a mound. *J. Waterway, Port, Coastal and Ocean Engng ASCE* 115(2), pp. 269-284

Vogel, J.A., Radder, A.C. and de Reus, J.H. 1988. Verification of numerical wave propagation models in tidal inlets. *Proc. 21st Coastal Eng. Conf. ASCE, Malaga,* pp. 433-447.